

# Topological Origin of Geophysical Waves

Pierre Delplace<sup>1</sup>, J. B. Marston<sup>2</sup>, Antoine Venaille<sup>1</sup>

November 21, 2022

Symmetries and topology are central to an understanding of physics. Topology explains the precise quantization of the Hall effect [1, 2, 3] and the protection of surface states in topological insulators against scattering by non-magnetic impurities or bumps [4]. Subsequent to the discovery of the quantum spin Hall effect [5, 6, 7, 8], states of matter with different topological properties were classified according to the discrete symmetries of the system [9, 10]. Recently topologically protected edge excitations have been found in artificial lattice structures that support classical waves of various types [11, 12]. However, the interplay between discrete symmetries and the topology of fluid waves has so far played no role in the study of the dynamics of oceans and atmospheres. Here we show that, as a consequence of the rotation of the Earth that breaks time reversal symmetry, equatorially trapped Kelvin and Yanai waves [13, 14] have a topological origin, manifesting as equatorial edge modes in the rotating shallow water model. These unidirectional edge modes are guaranteed to exist by the non-trivial global structure of the bulk Poincaré modes encoded through the first Chern number of value  $\pm 2$ , in agreement with the correspondence between behavior deep in the bulk and edge excitations of a physical system. Thus the oceans and atmospheres of Earth and other rotating planets naturally share fundamental properties with topological insulators, despite the absence of an underlying lattice. As equatorially trapped Kelvin waves are an important component of El Niño Southern Oscillation [15], and Madden-Julian Oscillation [16], our results demonstrate the topology plays an unexpected role in Earth's climate system. These and other geophysical waves of topological origin are protected against static perturbations by time scale separation from other modes that inhibits scattering.

A minimal model for equatorial waves is given by the rotating shallow water equations [17, 18] that describe the dynamics of a thin layer of fluid on a two-dimensional surface of height  $h(\mathbf{x}, t)$  and horizontal velocity  $\mathbf{u}(\mathbf{x}, t)$

$$\partial_t h + \nabla \cdot (h\mathbf{u}) = 0, \quad (1)$$

$$\partial_t \mathbf{u} + (\mathbf{u} \cdot \nabla) \mathbf{u} = -g \nabla h - f \hat{\mathbf{n}} \times \mathbf{u}. \quad (2)$$

The Coriolis parameter  $f = 2\boldsymbol{\Omega} \cdot \hat{\mathbf{n}}$  is twice the projection of the planetary angular rotation vector on the local vertical axis  $\hat{\mathbf{n}}$  and  $g$  is the constant of gravitational acceleration. When linearized about a state of rest ( $\mathbf{u} = 0$ ) and mean height ( $h = H$ ), this dynamical system may be rewritten as an independent particle Schrödinger-like equation  $i\partial_t \Psi = \mathcal{H}\Psi$ , where  $\Psi = (\mathbf{u}, \eta)$  is a triplet of fields describing the two components of the perturbed velocity field and the perturbed height

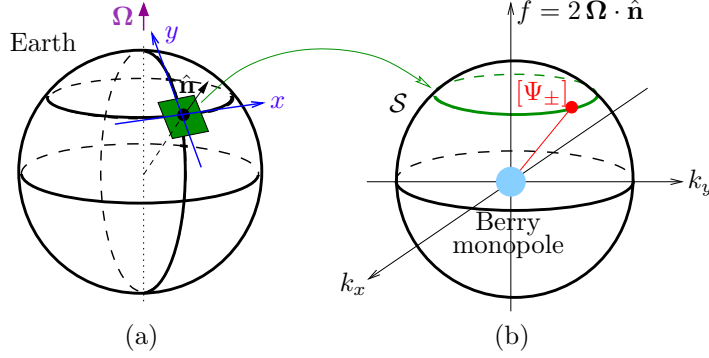


Figure 1: (a) Relation between the spherical geometry of a rotating planet and the unbounded  $f$ -plane geometry (b) Parameter space for the eigenmodes on the unbounded  $f$ -plane geometry.

field  $\eta$ , and where  $\mathcal{H}$  is a Hermitian operator (see Methods). Because the fields  $(\mathbf{u}, \eta)$  are real,  $\mathcal{H}$  is equal to the negative of its complex conjugate:  $\Xi \mathcal{H} \Xi^{-1} = -\mathcal{H}$  where  $\Xi$  is the operator that effects complex conjugation, with  $\Xi^2 = 1$ . In the quantum context, the operation is referred to as a particle-hole transformation because it inverts the spectrum. Moreover, time reversal symmetry  $t \rightarrow -t$ ,  $\mathbf{x}' \rightarrow \mathbf{x}$ ,  $\eta \rightarrow \eta$ ,  $\mathbf{u} \rightarrow -\mathbf{u}$  is broken by non-zero Coriolis parameter  $f \neq 0$  in Eq. (2). The broken symmetry generates gaps in the shallow water spectrum [18].

According to the classification of gapped Hamiltonians [10, 9], operator  $\mathcal{H}$  belongs to the symmetry class with Cartan label D [19]. In two dimensions class D implies that some of the wavefunctions  $\Psi$  should exhibit non-trivial topological properties that are characterized by an integer that we elucidate below. In solids, the topological indices correspond to the first Chern number of fiber bundles of Bloch eigenstates in the Brillouin zone [20] with each energy band characterized by a topological number. By contrast the shallow water model has no underlying lattice and therefore no Brillouin zone. We therefore use a different approach to investigate the topology of the system, by considering eigenmodes of the shallow water equations for a continuous family of  $f$ -plane configurations.

The  $f$ -plane approximation commonly used in geophysics [18] amounts to the neglect of Earth sphericity by assuming that the dynamics take place on a tangent plane with constant  $f$ , see Fig. 1(a). Translational symmetry ensures that eigenmodes of the linearized dynamics in this geometry are on the form  $\hat{\Psi} \exp(i\omega t - ik_x x - ik_y y)$  where  $\hat{\Psi}$  has three components. Viewing  $f/c$  as an external parameter, where  $c = \sqrt{gH}$  is the speed of non-rotating shallow water gravity waves, the eigenmodes may be easily found at each point in the space  $(k_x, k_y, f/c)$  as depicted in Fig. 1(b). There are 3 bands with frequencies  $\omega_{\pm} = \pm (f^2 + c^2 k^2)^{1/2}$  and  $\omega_0 = 0$  where  $k^2 \equiv k_x^2 + k_y^2$ , with corresponding wavefunctions  $\{\Psi_{\pm}, \Psi_0\}$ . For  $f \neq 0$ , the bands separate gaps of frequency  $f$  (Fig. 2). The zero-frequency modes are in geostrophic balance; the other two modes are Poincaré waves with dispersions  $\omega_{\pm}$  that are particle-hole symmetric about zero frequency.

Eigenmodes depend on the triplet of parameters  $(k_x, k_y, f/c)$ , that correspond to the set of waves in all possible  $f$ -plane configurations. The eigenmodes do not vary with the distance from the origin in  $(k_x, k_y, f/c)$ -space and can therefore be parameterized on the surface of a sphere  $\mathcal{S}$  that encloses the singular band-crossing point at the origin  $(k_x, k_y, f/c) = (0, 0, 0)$  [see Fig. 1 b) and Methods]. Each of the eigenstates  $\{\Psi_-, \Psi_0, \Psi_+\}$  defines a fiber bundle over  $\mathcal{S}$  that may possess topological defects.

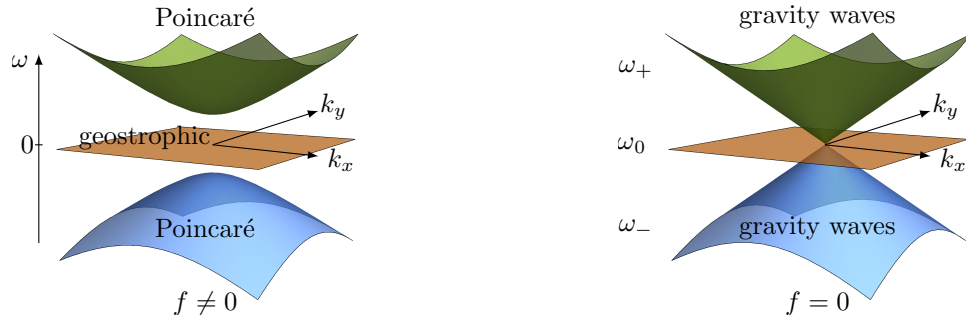


Figure 2: Dispersion relation in unbounded  $f$ -plane geometry. (a) Rotating  $f \neq 0$ ; and (b) non-rotating  $f = 0$ .

The singularities reflect the impossibility of continuously defining the eigenmodes everywhere on the sphere. They are quantified by the first Chern number that equals the quantized Berry flux generated by a (Berry) monopole located at the center of  $\mathcal{S}$ , where the three bands cross [21, 20]. The singularity is analogous to the one exhibited by an electron wavefunction that cannot be defined continuously around a Dirac magnetic monopole. [22]. We find  $\{\Delta\mathcal{C}_-, \Delta\mathcal{C}_0, \Delta\mathcal{C}_+\} = \{-2, 0, 2\}$  [see Methods]. Only the Poincaré modes  $\Psi_{\pm}$  are topologically non-trivial as the geostrophic modes  $\Psi_0$  have zero Chern index.

According to the bulk-edge correspondence, a striking physical consequence of the singularities is the existence of robust unidirectional (chiral) edge modes at the interface between two domains of opposite  $f$  [20]. Such an interface is naturally realized at the equator of a rotating planet. For any frequency that lies within the bulk gaps, the number of topological edge states is fixed by the set of Chern numbers [23]. When  $\Delta\mathcal{C}_{\pm} = \pm 2$  there are two extra unidirectional edge modes in the frequency gaps.

To study the edge waves, we numerically diagonalize the linearized shallow-water equations on a lattice, making  $f$  vary in one direction. For simplicity we adopt a planar geometry with periodic boundary conditions (Fig. 3). The use of the torus comes with a price as there are now two equators with opposite orientations [24]. In accordance with the Chern number calculation, we find that each equator supports two chiral edge modes in addition to quasi-geostrophic planetary Rossby waves. The spectrum is similar to the classical dispersion of shallow water waves on an equatorial beta-plane or on a sphere, see for instance [17, 25, 18], allowing us to identify the two topological edge states as Kelvin and Yanai modes, both of which have been observed in Earth atmosphere [16] and oceans [15]. They differ qualitatively from other edge modes – now seen to be equatorially trapped Rossby waves – that are not topologically protected. We have verified that Yanai and Kelvin waves bridge the whole frequency gap regardless of the precise shape of  $f(y)$ . Kelvin waves connect the positive and negative frequency Poincaré bands, while Yanai waves connect both Poincaré bands to the quasi-geostrophic band. By contrast, Rossby modes are now be seen to be geostrophic modes with the zero-frequency degeneracy lifted by the presence of the gradient in  $f$  (the so-called  $\beta$ -plane effect).

We stress one important point concerning the role of the spherical geometry of the planet in the approach followed in this paper. We removed any effect of this sphericity by considering the  $f$ -plane approximation. However, the construction of the sphere  $\mathcal{S}$  in parameter  $(k_x, k_y, f/c)$  restores

some sphericity to the problem by taking into account the effect of varying  $f$  on the eigenmodes of the shallow water equations. Topology then shows that the existence of Yanai and Kelvin wave is not due to the geometry of the Earth, but rather is a result of the change in sign of the Coriolis parameter, a result that cannot be obtained in classical calculations performed using the equatorial beta plane approximation that linearizes the curvature of the Earth away from the equator [17, 25, 18].

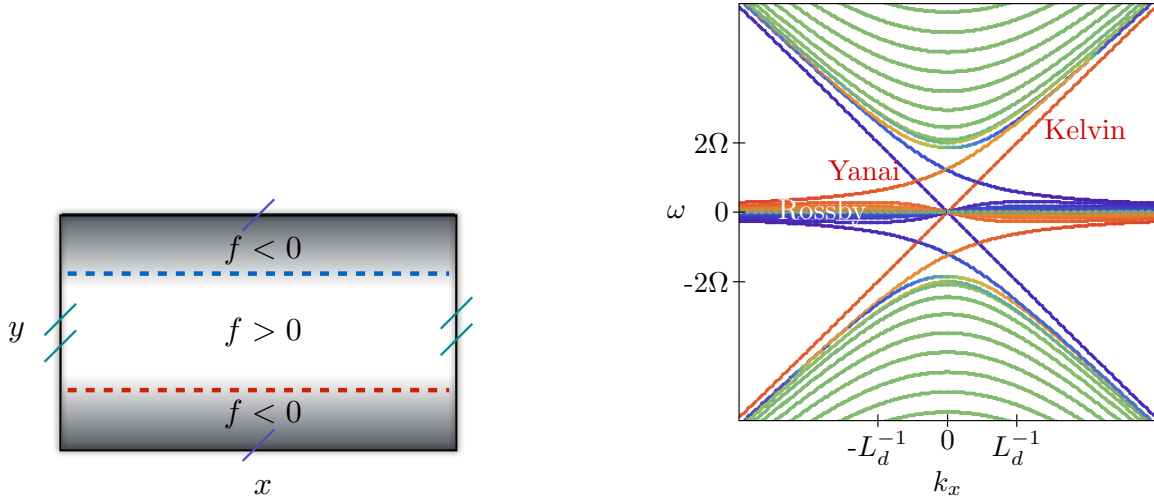


Figure 3: (a) A plane that is periodic in both the  $x$ - and  $y$ -directions. The Coriolis parameter  $f$  varies between  $\pm 2\Omega$ . The region with  $f = 2\Omega$  (white) is separated from another with  $f = -2\Omega$  by two narrow equatorial regions over which  $f(y)$  interpolates smoothly. (b) Dispersion relation for modes obtained by numerical diagonalization of the linearized shallow water model on a lattice.  $L_d = c/2\Omega$  is the Rossby radius of deformation. The delocalized bulk modes are marked in green, edge states localized around the earth-like equator are red, and edge states localized on the other equator are blue. See Methods for details and parameters.

Other ideas from topology have been used in hydrodynamics [26, 27, 28], but have so far never been applied to fluid waves. While the dispersion relations of a variety of fluid waves are well known, the peculiar topological properties of the corresponding eigenmodes that may emerge as a consequence of broken discrete symmetries have not previously been explored. As discussed above, the shallow water system exhibits particle-hole symmetry stemming from the fact that the velocity and displacement fields are real-valued. Any linearized fluid flow model, such as the rotating shallow water model, that breaks time reversal symmetry will belong to class D. We expect that other systems, from laboratory to geophysical to astrophysical scales may exhibit waves that owe their existence to topology. This is remarkable, as the only previously known physical system to belong to class D are chiral  $p$ -wave superconductors [29, 20], for which experimental confirmation remains under debate.

Our results permit a new understanding of rotating shallow water waves based upon topology, with the Poincaré and quasi-geostrophic modes carrying different topological indices. The celebrated Yanai and Kelvin waves emerge as topologically protected modes at the equatorial boundary of the two hemispheres of the rotating planet. In this picture the interiors of the northern, and the southern, hemispheres are two different topological phases with opposing Coriolis parameter. For frequencies between the Rossby and Poincaré wave bands, the only waves are those of topological

origin. Their energy can only propagate eastward along the equator, a property that is protected against static perturbations such as topography (see Methods). It will be interesting to investigate the resilience of topological waves against dissipation and non-linear wave-wave scattering processes.

<sup>1</sup> Univ Lyon, Ens de Lyon, Univ Claude Bernard, CNRS, Laboratoire de Physique, F-69342 Lyon, France

<sup>2</sup> Department of Physics, Box 1843, Brown University, Providence, RI 02912-1843 USA.

**Acknowledgements** We thank David Carpentier, Baylor Fox-Kemper, Thibaud Louvet, and Steve Tobias for discussions.

**Author Contributions** The authors contributed equally to all aspects (theoretical and numerical) of the paper.

**Author Information** The authors declare no competing financial interests.

## References

- [1] R. B. Laughlin, “Quantized Hall conductivity in two-dimensions,” Physical Review B, vol. 23, no. 10, pp. 5632–5733, 1981.
- [2] B. I. Halperin, “Quantized Hall Conductance, Current-Carrying Edge States, and the Existence of Extended States in a Two-Dimensional Disordered Potential,” Physical Review B, vol. 25, no. 4, pp. 2185–2190, 1982.
- [3] D. J. Thouless, M. Kohmoto, M. P. Nightingale, and M. Denny, “Quantized Hall Conductance in a Two-Dimensional Periodic Potential,” Physical Review Letters, vol. 49, no. 6, pp. 405–408, 1982.
- [4] M. Z. Hasan and C. L. Kane, “Colloquium: Topological insulators,” Reviews of Modern Physics, vol. 82, pp. 3045–3067, Nov. 2010.
- [5] C. L. Kane and E. J. Mele, “Quantum spin Hall effect in graphene,” Physical Review Letters, vol. 95, no. 22, p. 226801, 2005.
- [6] C. L. Kane and E. J. Mele, “ $Z_2$  topological order and the quantum spin Hall effect,” Physical Review Letters, vol. 95, no. 14, p. 146802, 2005.
- [7] B. A. Bernevig, T. L. Hughes, and S.-C. Zhang, “Quantum spin Hall effect and topological phase transition in HgTe quantum wells,” Science, vol. 314, no. 5806, pp. 1757–1761, 2006.
- [8] M. König, S. Wiedmann, C. Brüne, A. Roth, H. Buhmann, L. W. Molenkamp, X.-L. Qi, and S.-C. Zhang, “Quantum spin Hall insulator state in HgTe quantum wells,” Science, vol. 318, no. 5851, pp. 766–770, 2007.
- [9] S. Ryu, A. P. Schnyder, A. Furusaki, and A. W. Ludwig, “Topological insulators and superconductors: tenfold way and dimensional hierarchy,” New Journal of Physics, vol. 12, no. 6, p. 065010, 2010.

- [10] A. Kitaev, “Periodic table for topological insulators and superconductors,” arXiv preprint arXiv:0901.2686, 2009.
- [11] L. Lu, J. D. Joannopoulos, and M. Soljačić, “Topological photonics,” Nature Photonics, vol. 8, no. 11, pp. 821–829, 2014.
- [12] S. D. Huber, “Topological mechanics,” Nature Physics, vol. 12, no. 7, pp. 621–623, 2016.
- [13] T. Matsuno, “Quasi-Geostrophic Motions in the Equatorial Area,” Journal of the Meteorological Society of Japan. Ser. II, vol. 44, no. 1, pp. 25–43, 1966.
- [14] M. S. Longuet-Higgins, “The Eigenfunctions of Laplace’s Tidal Equations over a Sphere,” Philosophical Transactions of the Royal Society of London A: Mathematical, Physical and Engineering Sciences, vol. 262, pp. 511–607, Feb. 1968.
- [15] L. Miller, R. E. Cheney, and B. C. Douglas, “GEOSAT altimeter observations of Kelvin waves and the 1986-87 El Niño,” Science, vol. 239, no. 4835, p. 52, 1988.
- [16] M. Wheeler and G. N. Kiladis, “Convectively coupled equatorial waves: Analysis of clouds and temperature in the wavenumber–frequency domain,” Journal of the Atmospheric Sciences, vol. 56, no. 3, pp. 374–399, 1999.
- [17] A. E. Gill, Atmosphere-Ocean Dynamics, vol. 30. Academic Press, 1982.
- [18] G. Vallis, Atmospheric and oceanic fluid dynamics: fundamentals and large-scale circulation. Cambridge, U.K.: Cambridge University Press, 2nd ed., 2017.
- [19] A. Altland and M. R. Zirnbauer, “Nonstandard symmetry classes in mesoscopic normal-superconducting hybrid structures,” Physical Review B, vol. 55, no. 2, p. 1142, 1997.
- [20] B. A. Bernevig and T. L. Hughes, Topological insulators and topological superconductors. Princeton University Press, 2013.
- [21] M. V. Berry, “Quantal phase factors accompanying adiabatic changes,” Proceedings of the Royal Society of London A: Mathematical, Physical and Engineering Sciences, vol. 392, no. 1802, pp. 45–57, 1984.
- [22] P. A. M. Dirac, “Quantised singularities in the electromagnetic field,” Proceedings of the Royal Society of London A: Mathematical, Physical and Engineering Sciences, vol. 133, no. 821, pp. 60–72, 1931.
- [23] Y. Hatsugai, “Chern number and edge states in the integer quantum Hall effect,” Physical Review Letters, vol. 71, no. 22, p. 3697, 1993.
- [24] E. S. Warneford and P. J. Dellar, “Thermal shallow water models of geostrophic turbulence in Jovian atmospheres,” Physics of Fluids, vol. 26, no. 1, 2014.
- [25] N. Paldor, Shallow Water Waves on the Rotating Earth. Springer, 2015.
- [26] V. I. Arnold and B. A. Khesin, Topological methods in hydrodynamics, vol. 125. Springer Science & Business Media, 1999.
- [27] H. K. Moffatt, “The topology of turbulence. Lesieur, M (ed.) et al., Ecole de Physique des Houches UJF INPG Grenoble,” Les Houches session LXXIV, vol. 31, 2001.

- [28] D. Kleckner and W. T. M. Irvine, “Creation and dynamics of knotted vortices,” Nature physics, vol. 9, no. 4, pp. 253–258, 2013.
- [29] G. E. Volovik, The universe in a helium droplet, vol. 117. Oxford University Press on Demand, 2003.

## Methods: Topological Origin of Geophysical Waves

### 1 First Chern Number of Shallow Water Eigenmodes

We consider flows on a  $f$ -plane with  $x$  in the zonal direction (positive towards the East) and  $y$  the meridional direction (positive towards North) [see Figure 1(a) in the Main Text]. The velocity field is denoted by  $\mathbf{u}(\mathbf{x}, t) = (u(\mathbf{x}, t), v(\mathbf{x}, t))$ , with  $\mathbf{x} = (x, y)$ . The value of the Coriolis parameter  $f$  is spatially constant, but will be considered as an external parameter that can be varied between  $\pm 2\Omega$ , where  $\Omega$  is the planet rotation rate. The extremal values correspond to the value of  $f$  at the Northern and Southern pole. The system possess one intrinsic time scale  $1/2\Omega$  and one intrinsic length scale given by the global Rossby radius of deformation  $L_d$  along with a speed  $c$ :

$$L_d = \frac{c}{2\Omega}, \quad c = \sqrt{gH}. \quad (\text{S1})$$

The dynamics (1)-(2) can then be expressed in terms of dimensionless quantities

$$\tilde{\eta} = \frac{h - H}{H}, \quad \tilde{\mathbf{u}} = \frac{\mathbf{u}}{c}, \quad \tilde{t} = 2\Omega t, \quad \tilde{f} = \frac{f}{2\Omega}, \quad \tilde{\mathbf{x}} = \frac{\mathbf{x}}{L_d}, \quad (\text{S2})$$

and the linearized equations of motion around a state at rest ( $\mathbf{u} = 0$ ,  $h = H$ ) read

$$\partial_{\tilde{t}} \tilde{\eta} = -\partial_{\tilde{x}} \tilde{u} - \partial_{\tilde{y}} \tilde{v} \quad (\text{S3})$$

$$\partial_{\tilde{t}} \tilde{u} = -\partial_{\tilde{x}} \tilde{\eta} + \tilde{f} \tilde{v}, \quad (\text{S4})$$

$$\partial_{\tilde{t}} \tilde{v} = -\partial_{\tilde{y}} \tilde{\eta} - \tilde{f} \tilde{u}. \quad (\text{S5})$$

For convenience, we drop the  $\sim$  tilde in the following.

Eigenmodes (equivalently, normal modes) are propagating planar waves. Let  $\hat{\eta}$ ,  $\hat{u}$ ,  $\hat{v}$  be the amplitudes of the fields  $\eta$ ,  $u$ ,  $v$  for mode  $e^{i\omega t - ik_x x - ik_y y}$ . The amplitudes obey the eigenvalue equation:

$$\omega \begin{pmatrix} \hat{\eta} \\ \hat{u} \\ \hat{v} \end{pmatrix} = \begin{pmatrix} 0 & k_x & k_y \\ k_x & 0 & -if \\ k_y & if & 0 \end{pmatrix} \begin{pmatrix} \hat{\eta} \\ \hat{u} \\ \hat{v} \end{pmatrix}. \quad (\text{S6})$$

Diagonalization of this matrix leads to three eigenvalues corresponding to three wave bands in wavenumber-frequency space. The normalized eigenvectors associated with the positive frequency band  $\omega_+ = (k^2 + f^2)^{1/2}$  are

$$\Psi_+(k_x, k_y, f) = \frac{1}{\sqrt{2}} \begin{pmatrix} \frac{k}{\sqrt{k^2 + f^2}} \\ \frac{k_x}{k} - i \frac{f k_y}{k \sqrt{k^2 + f^2}} \\ \frac{k_y}{k} + i \frac{f k_x}{k \sqrt{k^2 + f^2}} \end{pmatrix} \quad (\text{S7})$$

The ones associated with the zero frequency band  $\omega_0 = 0$  are

$$\Psi_0(k_x, k_y, f) = \frac{1}{\sqrt{k^2 + f^2}} \begin{pmatrix} 1 \\ i \frac{k_y}{k} \\ -i \frac{k_x}{k} \end{pmatrix} \quad (\text{S8})$$



Eigenvectors for the negative frequency band  $\omega_- = -(k^2 + f^2)^{1/2}$  are easily obtained by taking advantage of the system symmetry:  $\Psi_-(k_x, k_y, f) = \Psi_+(-k_x, -k_y, -f)$ .

We calculate the Chern number of the fiber bundle defined by eigenvectors of the positive frequency wave band parameterized on the unit sphere in the space  $(k_x, k_y, f)$  [see Figure 1(b) in the Main Text]. Importantly, normalized eigenvectors  $(\Psi_0, \Psi_\pm)$  are defined only up to a phase. Here we show that this phase cannot be defined continuously for  $\Psi_\pm$  over all possible values of  $(k_x, k_y, f)$ . To see this, first notice that the eigenstates can be parametrized with the use of spherical coordinates. Introducing the colatitude  $\theta$  and the longitude  $\varphi$  (that should not be confused with colatitude and longitude on the planetary sphere in physical space), the normalized eigenvectors of the positive frequency wave band may be rewritten as:

$$\Psi_+ = \frac{1}{\sqrt{2}} \begin{pmatrix} \sin \theta \\ \cos \varphi - i \cos \theta \sin \varphi \\ \sin \varphi + i \cos \theta \cos \varphi \end{pmatrix}. \quad (\text{S9})$$

The eigenvectors are multivalued at  $\theta = 0$  and  $\theta = \pi$ , respectively the north and south poles of the parameter sphere  $\mathcal{S}$  shown in Fig. 1(b) of the Main Text. The multivaluedness is a topological property of the vector bundle that is defined as the set of  $\Psi_+$  over the base space  $(\theta, \varphi)$ . The multivaluedness can be quantified by non-vanishing first Chern number that we evaluate below.

Recalling that the eigenmodes are defined only up to a phase, a gauge transformation can be used to regularize the eigenmodes at one of the poles. In particular, we define

$$\Psi_+^N = \Psi_+ e^{i\varphi}, \quad \Psi_+^S = \Psi_+ e^{-i\varphi} \quad (\text{S10})$$

so that  $\Psi_+^N$  is a single-valued function of  $(\theta, \varphi)$  everywhere but at the south pole. Likewise  $\Psi_+^S$  is a single-valued function of  $(\theta, \varphi)$  everywhere but at the north pole. The Berry connections associated with these vector bundles are

$$\mathbf{A}_+^N = -i \langle \Psi_+^N, \nabla_s \Psi_+^N \rangle, \quad \mathbf{A}_+^S = -i \langle \Psi_+^S, \nabla_s \Psi_+^S \rangle \quad (\text{S11})$$

with the inner product defined for the 3-component amplitudes as  $\langle A, B \rangle \equiv A_1^* B_1 + A_2^* B_2 + A_3^* B_3$  and  $\nabla_s$  is the gradient operator on the unit sphere in  $(k_x, k_y, f)$  parameter space. These Berry connections are related by the gauge transformation through

$$\mathbf{A}_+^S = \mathbf{A}_+^N + 2\nabla_s \varphi. \quad (\text{S12})$$

At any point where  $\mathbf{A}_+^N$  and  $\mathbf{A}_+^S$  are not singular, the Berry curvature is given by

$$\mathbf{B}_+ = \nabla_s \times \mathbf{A}_+^N = \nabla_s \times \mathbf{A}_+^S. \quad (\text{S13})$$

The Chern number for the fiber bundle of eigenvectors with positive frequencies on the unit sphere in  $(k_x, k_y, f)$ -space is defined as the flux of the Berry curvature through  $\mathcal{S}$

$$\Delta \mathcal{C}_+ = \frac{1}{2\pi} \int_0^\pi d\theta \int_0^{2\pi} d\varphi \mathbf{B}_+ \cdot \mathbf{e}_k \quad (\text{S14})$$

where  $\mathbf{e}_k(\theta, \varphi)$  is the vector normal to the sphere pointing in the outward direction. Stokes theorem can be applied separately for each hemisphere of  $\mathcal{S}$  where the Berry connection is well defined,

e.g. along the equator circle ( $\theta = \pi/2$ ), with  $\mathbf{B}_+ = \nabla_s \times \mathbf{A}_+^N$  in the northern hemisphere and  $\mathbf{B}_+ = \nabla_s \times \mathbf{A}_+^S$  in the southern hemisphere. The calculation yields

$$\Delta\mathcal{C}_+ = \frac{1}{2\pi} \int_0^{2\pi} d\varphi (\mathbf{A}_+^N - \mathbf{A}_+^S) \cdot \mathbf{e}_\varphi. \quad (\text{S15})$$

Using Eq. (S12), we find  $\Delta\mathcal{C}_+ = 2$ . This Chern number can be interpreted as the topological invariant of the transition from one hemisphere to another for the case of the positive frequency eigenmodes of the shallow water model in the  $f$ -plane approximation, with  $f$  taken as an external parameter that tunes this transition. Note that we have derived this result by considering the fiber bundle of eigenmodes parameterized on the unit sphere, but it is straightforward to show that it holds on any sphere of radius  $\omega_+ > 0$  in  $(k_x, k_y, f)$  space since the normalized eigenvectors  $\Psi_+$  do not depend on  $\omega_+$ . Similar calculations show that the Chern number for the negative frequency eigenmodes is  $\Delta\mathcal{C}_- = -2$ , and  $\Delta\mathcal{C}_0 = 0$  for the zero-frequency eigenmodes.

The number of topological edge states at the interface between two domains of opposite  $f$  is fixed by the set of Chern numbers  $\{\Delta\mathcal{C}_-, \Delta\mathcal{C}_0, \Delta\mathcal{C}_+\}$ , according to bulk-edge correspondence [1, 2]. Let  $N_{\text{right}}^{\text{above}} - N_{\text{left}}^{\text{above}}$  be the difference in the number of right-moving and left-moving modes in the gap above the central geostrophic band, and  $N_{\text{right}}^{\text{below}} - N_{\text{left}}^{\text{below}}$  be the difference in the number of right-moving and left-moving modes in the gap below. Bulk-edge correspondence then states that  $|\Delta\mathcal{C}| = \left| \left( N_{\text{right}}^{\text{above}} - N_{\text{left}}^{\text{above}} \right) - \left( N_{\text{right}}^{\text{below}} - N_{\text{left}}^{\text{below}} \right) \right|$ . The imbalance between right-moving and left-moving modes within the gap above the geostrophic band is quantified by  $N_{\text{right}}^{\text{above}} - N_{\text{left}}^{\text{above}}$ . Both numbers can vary with frequency within the gap, but their difference corresponds to the number of topologically protected chiral edge modes. In the present case, Chern number  $\Delta\mathcal{C}_0 = 0$  means that there are equal numbers of topological edge states with the same chirality in the gaps above and below the central band of geostrophic modes. Since there is no gap above the positive frequency band, and no gap below the negative frequency band, the number of chiral edge states in each gap surrounding the central band is given by  $|\Delta\mathcal{C}_\pm| = 2$ .

## 2 Numerical Calculation of Eigenmodes With $f(y)$ : From the Shallow Water Model to a Haldane-like Model on the Lieb lattice

The linearized rotating shallow water dynamics on a doubly periodic domain with  $f$  varying in the  $y$  direction is solved numerically using a standard C-grid discretization procedure [3]. This approach also establishes a direct link with usual lattice models in condensed matter physics.

The domain is discretized into a uniform grid with  $N_x \times 2N_y$  cells located at  $(x, y) = (m\delta x, n\delta y)$  where  $\delta x$  and  $\delta y$  are the size of the grid cells, and  $m$  and  $n$  are integers. Assuming time-harmonic solutions, eigenmodes of the discretized shallow water system are described at each grid point by the real part of the triplet  $e^{i\omega t}(h_{m,n}, \mathbf{u}_{m,n})$ . Following the C-grid discretization procedure, the system of equations (S3)-(S4)-(S5) then turns into an eigenvalue problem for the fields  $(h(m, n, \omega), \mathbf{u}(m, n, \omega))$ :

$$\omega u_{m,n} = -t_x (h_{m-1,n} - h_{m,n}) - \frac{if}{4} (v_{m,n} + v_{m,n+1} + v_{m-1,n} + v_{m-1,n+1}) \quad (\text{S16a})$$

$$\omega v_{m,n} = -t_y (h_{m,n-1} - h_{m,n}) + \frac{if}{4} (u_{m,n} + u_{m+1,n} + u_{m+1,n-1} + u_{m,n-1}) \quad (\text{S16b})$$

$$\omega h_{m,n} = t_x (u_{m,n} - u_{m+1,n}) + t_y (v_{m,n} - v_{m,n+1}) \quad (\text{S16c})$$

where the change of variable  $ih \rightarrow h$  was performed for convenience, and where we have defined  $t_x = \frac{1}{\delta x}$  and  $t_y = \frac{1}{\delta y}$ . We consider a meridional dependence of the Coriolis parameter through the map  $f_y$  that we specify below. This allows us to treat arbitrary variations of  $f$ , and in particular any equator-like interface from  $f < 0$  to  $f > 0$ . For concreteness, we consider periodic boundary conditions in the  $y$  direction with  $n$  running from 1 to  $2N_y$ , and we choose

$$f_n = \tanh\left((n-1)\frac{\delta y}{R_f}\right) - \tanh\left((n-N_y)\frac{\delta y}{R_f}\right) + \tanh\left((n-2N_y)\frac{\delta y}{R_f}\right) \quad (\text{S17})$$

where  $R_f$  gives the scale of variation for the gradient of the Coriolis parameter in the  $y$  direction. There are two regions with opposite  $f$  and two interfaces between the regions (see Figure S1).

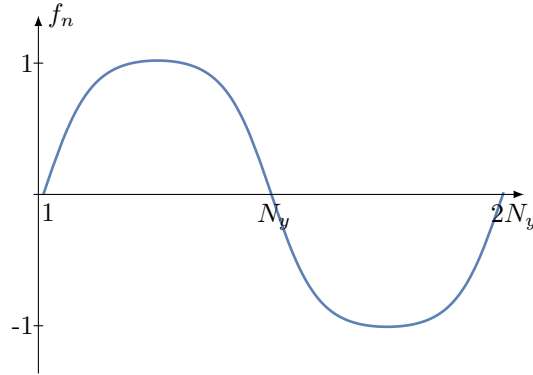


Figure S1: Variation of the Coriolis parameter as a function of  $n$  for  $N_y = 50$  and  $R_f/\delta y = 10$ .

The frequency  $\omega$  is the eigenvalue of a tight-binding model on the Lieb lattice shown in Figure S2. Each site is coupled to its nearest neighbors by hopping parameters  $\pm t_x$  and  $\pm t_y$ . The minus sign that appears in these matrix elements can be interpreted as a phase of  $\pi$  picked up when hopping from site to site. While this phase does not break time-reversal symmetry, the coupling  $\pm if/4$  that accounts for a phase of  $\pm\pi/2$  accumulated between second nearest neighbors, does. The total phase accumulated around a unit cell is a multiple of  $2\pi$ , so that the net flux through the system vanishes. This behavior is analogous to the seminal Haldane model on the honeycomb lattice, the archetypal example of a topological Chern insulator in the absence of an applied magnetic field [4].

Because of translational invariance, the Fourier transformed fields  $(h(k_x, n, \omega), \mathbf{u}(k_x, n, \omega))$  satisfy

$$\omega u_{k_x,n} = -t_x (e^{-ik_x\delta x} - 1) h_{k_x,n} - i\frac{f_n}{4} (1 + e^{-ik_x\delta x}) (v_{k_x,n} + v_{k_x,n+1}) \quad (\text{S18a})$$

$$\omega v_{k_x,n} = -t_y (h_{k_x,n-1} - h_{k_x,n}) + i\frac{f_n}{4} (1 + e^{ik_x\delta x}) (u_{k_x,n-1} + u_{k_x,n}) \quad (\text{S18b})$$

$$\omega h_{k_x,n} = t_x (1 - e^{ik_x\delta x}) u_{k_x,n} + t_y (v_{k_x,n} - v_{k_x,n+1}) . \quad (\text{S18c})$$

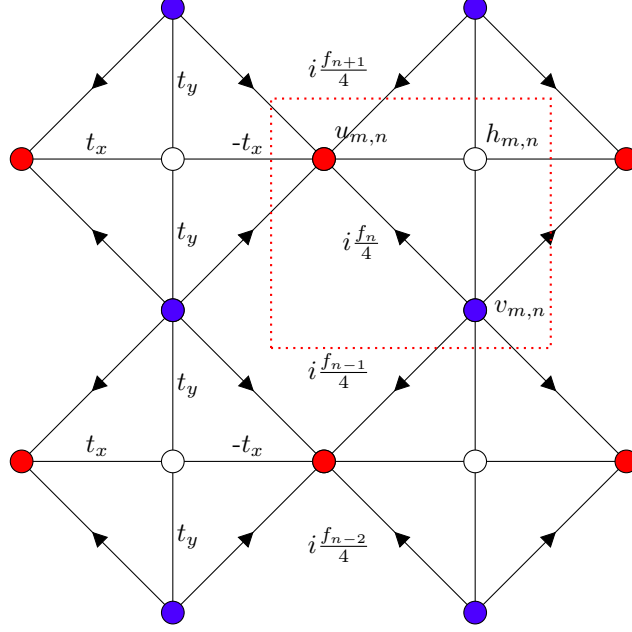


Figure S2: Lieb lattice representing the coupling between the three fields of the discretized rotating shallow water model following the C-grid procedure. The field  $u(m,n)$  is represented by a red dot,  $v(m,n)$  by a blue dot and  $h(m,n)$  by a white dot. A unit cell is highlighted by a red dashed rectangle. The nearest neighbors are coupled by  $\pm t_x$  and  $\pm t_y$  hopping terms, and the second nearest neighbors by an imaginary terms proportional to the Coriolis parameter  $f$  that breaks time-reversal symmetry. Arrows indicate directions along which phase  $+\pi/2$  is picked up.

There are four dimensionless parameters given by  $R_f/L_y$ ,  $L_d/L_y$ ,  $L_x/L_y$ , and  $\delta y/L_y$ . The first parameter controls the interface thickness between regions of constant (but opposite)  $f$ . It is of order 1 for a spherical geometry, but the difference between non-topological and topological edge modes is revealed by considering a sharper interface, with  $R_f/L_y \approx 0.1$ . The second non-dimensional parameter  $L_d/L_y$  controls the intrinsic length scale of the domain with respect to the domain size. It is of order one in the atmosphere, and of order 0.1 in the ocean. The third parameter  $L_x/L_y$  is a geometric parameter, of order one for the atmosphere and oceans on Earth. For convenience, we consider  $L_x/L_y \gg 1$ , which yields continuous lines  $\omega(k_x)$  in the dispersion relation. The last parameter is related to the discretization of the continuous problem and is chosen such that  $\delta y/L_y \ll R_f/L_y$  and  $\delta y/L_y \ll L_d/L_y$ . The precise form of the dispersion relation for  $k_x \sim \pm 2\pi/\delta y$  depends on the choice of the discrete geometry. However, for a given  $k_x$ , the dispersion relation of the continuous shallow water system is recovered in the limit  $\delta x \rightarrow 0$ .

The system (S18) is diagonalized numerically. The frequency spectrum shown in Fig 3 of the Main Text is obtained for  $N_y = 50$ ,  $R_f/\delta y = 10$  and Rossby radius of deformation  $L_d = R_f/2$ . We checked that whatever the value of those the dimensionless parameters, the gaps obtained for  $f \neq 0$  are filled by two equatorially trapped modes, and that for each equator, the difference of right-moving to left moving edge modes within the frequency gaps where equal to  $\pm 2$ . In contrast, the amplitude in frequency of the Rossby waves or the emergence of equatorially trapped Poincaré waves depend on the shape of  $f(y)$ .

### 3 Scattering of Equatorial Kelvin Waves by a Static Perturbation

Equatorial Kelvin waves are observed in Earth oceans [5] and atmosphere [6]. The waves are reproduced by models more general than the single-layer shallow water equations considered in the Main Text [7]. Conversion of low-frequency eastward-moving Kelvin waves to westward Rossby waves can occur at the eastern margins of ocean basins [3] or by scattering from topography [8, 9]. Here we investigate the frequency dependence of the scattering of equatorial Kelvin waves by a region of enhanced stratification in a 2-layer primitive equation model [10, 11] to demonstrate that Kelvin waves that oscillates at an intermediate frequency in the gap between the Rossby and Poincaré waves are not backscattered by the perturbation.

The model is defined on a spherical geodesic grid [12] and is described in Ref. [13]. This minimal model of the general circulation describes fluid motion in the horizontal within each layer, flow between the layers, and the variation of temperature within each layer. The model has rigid upper and lower lids and supports internal waves at the interface between the two layers. The temperature field is advected by the fluid and acts back upon it via pressure as determined by the equation of state for an ideal gas and hydrostatic balance. There are in total 5 independent dynamical fields once the incompressibility of the fluid has been taken into account. The idealized model can be used to describe either a planetary atmosphere or an ocean that covers the whole planet. Code that implements the model is publicly available<sup>1</sup>.

The vertical mean temperature is initially uniform over the sphere, and can be set to zero without loss of generality. Stable stratification is imposed by setting the temperature of the upper layer to be 1 K greater than that of the lower layer, except in a region centered on the equator at longitude 90° W (indicated by the dashed circles in Figure S3) where the temperature difference increases up to a maximum of 10 K further with a Gaussian profile of width 20°. The lower layer is thus denser than the upper layer and supports internal Kelvin and Rossby waves that move at speeds comparable to those observed in the equatorial Pacific ocean. Waves can scatter off the region of enhanced stability because the wave speed is higher in that region. Kelvin waves in the ocean can be observed from satellite via surface altimetry as water that warms also expands. The imposed model stratification means that the simulated vertical mean temperature likewise serves as a proxy for the interface height.

Wavepackets are generated early in the simulations by adding a forcing term to the tendency of the difference  $\delta$  in the divergence of the velocity field between the two layers

$$\frac{\partial}{\partial t}\delta = \dots + A g_{10^\circ}(\theta - \pi/2) g_{\pi/m}(\phi - \omega t/m - \pi/m) \sin(\omega t - m\phi) \quad (\text{S19})$$

where  $\dots$  denotes the other terms in the equation of motion (Equation 5 of Ref. [?]) and  $g_\Delta(\alpha) \equiv \exp[-(\alpha/\Delta)^2]$  is a Gaussian of unit height centered at  $\alpha = 0$  and of width  $\Delta$ . The added driving acts for only half of an oscillation period, from  $t = 0$  to  $t = \pi/\omega$ . We choose  $A = 10^{-4} (\text{day})^{-1}$ , an amplitude sufficiently small for the waves to behave linearly. Apart from the wave driving term at the early stage of simulation, all other forcing terms and friction are turned off for the numerical experiments performed here.

---

<sup>1</sup>The application “GCM” is available for macOS 10.9 and higher on the Apple Mac App Store at URL <http://appstore.com/mac/gcm>

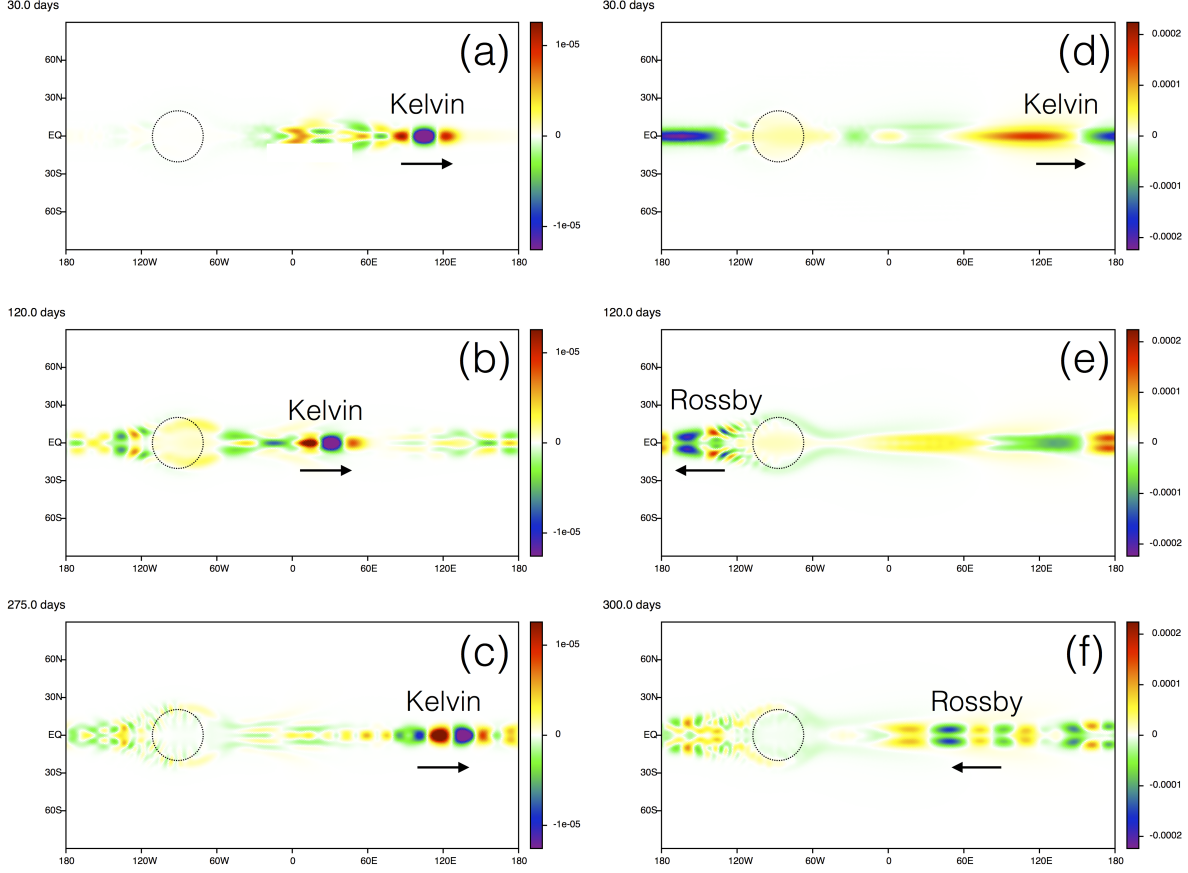


Figure S3: Simulated scattering of equatorial Kelvin waves. The region of enhanced stability is indicated by the dashed circle. The temperature of the upper layer in that region is enhanced by up to 10K above an otherwise uniform value of 1 K over that of the lower layer. The color scale displays the vertical mean temperature. (a) An intermediate frequency ( $\omega \approx 1 \text{ (day)}^{-1}$ ) eastward Kelvin wave packet at time  $t = 30$  days prior to interaction. The arrow indicates the direction of propagation. (b) By 120 days the intermediate frequency Kelvin wave has passed through the region of enhanced stability intact. (c) After 275 days the Kelvin wave has passed through the scattering region twice yet remains coherent. (d) A low-frequency ( $\omega \approx 0.2 \text{ (day)}^{-1}$ ), long-wavelength Kelvin wave at time  $t = 30$  days, prior to interaction, moves eastward. (e) At 120 days the low-frequency Kelvin wave strongly interacts with the region of enhanced stability, and generates westward moving Rossby waves. The Rossby waves are bimodal across the equator [3]. (f) By 300 days the Kelvin wave packet has been converted to Rossby waves that continue propagating westward.

An intermediate frequency wave train that consists largely of an eastward moving Kelvin wave is produced by setting the angular frequency  $\omega = 1 \text{ (day)}^{-1}$  and wavenumber  $m = 10$  [Figure S3(a)].<sup>2</sup> A low frequency, long wavelength Kelvin wave is created by choosing instead  $\omega = 0.2 \text{ (day)}^{-1}$  and  $m = 2$  [Figure S3(d)]. (Yanai waves can be generated by modifying the forcing term in Eq. S19 to be antisymmetric with respect to the equator.)

<sup>2</sup>Videos of the two simulations may be viewed at URLs <https://vimeo.com/204597701> and <https://vimeo.com/204598091>.

The localized region of enhanced stability breaks translational symmetry; therefore wavenumber is not conserved. Because the perturbation is static in time, however, the frequencies of the waves passing through the region remain unchanged. The intermediate frequency Kelvin wave packet propagates at a frequency that lies in the gap between the Rossby and Poincaré waves. There are thus no available scattering channels that match its frequency, and it emerges from the interaction intact [Figure S3(b, c)]. (Reflection symmetry of the Kelvin wave about the equator blocks scattering into the Yanai wave.) Because the waves in the frequency gap have a topological origin, the absence of scattering is a manifestation of topological protection. By contrast there is a band of Rossby waves at low frequencies, and the low-frequency Kelvin wave is strongly disturbed by its interaction with the enhanced stratification [Figure S3(e)], producing Rossby waves. At late times, the low-frequency Kelvin wave has largely been converted to Rossby waves moving in the opposite (westward) direction [Figure S3(f)].

## References

- [1] Y. Hatsugai, “Chern number and edge states in the integer quantum Hall effect,” Physical Review Letters, vol. 71, no. 22, p. 3697, 1993.
- [2] B. A. Bernevig and T. L. Hughes, Topological insulators and topological superconductors. Princeton University Press, 2013.
- [3] B. Cushman-Roisin and J.-M. Beckers, Introduction to Geophysical Fluid Dynamics – Physical and Numerical Aspects. Elsevier, 2nd ed., 2011.
- [4] F. D. M. Haldane, “Model for a quantum Hall effect without Landau levels: Condensed-matter realization of the ”parity anomaly”, ” Physical Review Letters, vol. 61, pp. 2015–2018, Oct 1988.
- [5] L. Miller, R. E. Cheney, and B. C. Douglas, “GEOSAT altimeter observations of Kelvin waves and the 1986-87 El Niño,” Science, vol. 239, no. 4835, p. 52, 1988.
- [6] M. Wheeler and G. N. Kiladis, “Convectively coupled equatorial waves: Analysis of clouds and temperature in the wavenumber–frequency domain,” Journal of the Atmospheric Sciences, vol. 56, no. 3, pp. 374–399, 1999.
- [7] A. E. Gill, Atmosphere-Ocean Dynamics, vol. 30. Academic Press, 1982.
- [8] M. J. McPhaden and A. E. Gill, “Topographic scattering of equatorial Kelvin waves,” Journal of Physical Oceanography, vol. 17, no. 1, pp. 82–96, 1987.
- [9] A. J. Majda, R. R. Rosales, E. G. Tabak, and C. V. Turner, “Interaction of large-scale equatorial waves and dispersion of Kelvin waves through topographic resonances,” Journal of Atmospheric Sciences, vol. 56, no. 24, pp. 4118–4133, 1999.
- [10] E. N. Lorenz, “Energy and Numerical Weather Prediction,” Tellus, vol. XII, no. 4, pp. 364–373, 1960.
- [11] I. M. Held and M. J. Suarez, “A two-level primitive equation atmospheric model designed for climatic sensitivity experiments,” Journal of the Atmospheric Sciences, vol. 35, no. 2, pp. 206–229, 1978.

- [12] T. D. Ringler, R. P. Heikes, and D. A. Randall, “Modeling the atmospheric general circulation using a spherical geodesic grid: A new class of dynamical cores,” Monthly Weather Review, vol. 128, no. 7, pp. 2471–2490, 2000.
- [13] J. B. Marston, “Planetary Atmospheres as Nonequilibrium Condensed Matter,” Annual Review of Condensed Matter Physics, vol. 3, pp. 285–310, Mar. 2012.